Insulation Resistance Degradation in Ni-$BaTiO_3$ Multilayer Ceramic Capacitors

Donhang (David) Liu

ASRC Federal Space and Defense

Work performed for NASA Goddard Space Flight Center

Insulation resistance (IR) degradation in Ni-$BaTiO_3$ multilayer ceramic capacitors has been characterized by the measurement of both time to failure and direct-current (DC) leakage current as a function of stress time under highly accelerated life test conditions. The measured leakage current-time dependence data fit well to an exponential form, and a characteristic growth time τ_{SD} can be determined. A greater value of τ_{SD} represents a slower IR degradation process. Oxygen vacancy migration and localization at the grain boundary region results in the reduction of the Schottky barrier height and has been found to be the main reason for IR degradation in Ni-$BaTiO_3$ capacitors. The reduction of barrier height as a function of time follows an exponential relation of $\phi(t) = \phi(0)\mathrm{e}^{-2\mathrm{Kt}}$, where the degradation rate constant $K = K_0 e^{-\frac{E_k}{kT}}$ is inversely proportional to the mean time to failure (MTTF) and can be determined using an Arrhenius plot. For oxygen vacancy electromigration, a lower barrier height $\phi(0)$ will favor a slow IR degradation process, but a lower $\phi(0)$ will also promote electronic carrier conduction across the barrier and decrease the insulation resistance. As a result, a moderate barrier height $\phi(0)$ (and therefore a moderate IR value) with a longer MTTF (smaller degradation rate constant K) will result in a minimized IR degradation process and the most improved reliability in Ni-$BaTiO_3$ multilayer ceramic capacitors. **Dielectric degradation; ceramic capacitors; reliability; insulation resistance; barium titanate.**

I. INTRODUCTION

Insulation resistance (IR) degradation related to oxygen vacancy migration has been considered to be the primary cause of reliability degradation of multilayer ceramic capacitors (MLCCs) with base-metal electrodes (BMEs). The behavior is characterized by a slow increase in the leakage current under an applied direct-current (DC) field stress. In order to reveal IR degradation in a timely manner, MLCCs are often degraded under highly accelerated life test (HALT) conditions with different temperatures and applied voltages. Previous studies have shown that there are three possible factors related to the IR degradation of $BaTiO_3$-based BME MLCCs: the dielectric layer, the $BaTiO_3$ grain boundaries, and the Ni-$BaTiO_3$ internal electrode interfaces.[1-4]

Deliverable to NASA Electronic Parts and Packaging (NEPP) Program to be published on nepp.nasa.gov, paper published in the IEEE Transactions on Components, Packaging and Manufacturing Technology, Vol. 5, No. 1, January 2015.

Unlike traditional $BaTiO_3$-based MLCCs with precious-metal electrodes (PMEs), BME MLCCs are co-fired in a reducing atmosphere to avoid oxidation of the electrodes. Despite the re-oxidation process, there is still a significant amount of oxygen vacancies that are accommodated in the $BaTiO_3$ dielectric layers. The failure mechanism of BME MLCCs is thought to be dominated by the electromigration of oxygen vacancies through the grain boundaries in the dielectric layers.[5–8] Waser et al.[9-12] studied the IR degradation in ambient-fired $SrTiO_3$ ceramic and acceptor-doped single-crystal $SrTiO_3$. The results showed that IR degradation begins with oxygen vacancy electromigration toward the cathode with respect to time, field, and temperature. Segregation of defects and dopants is found at the grain boundaries during the sintering process and results in the formation of space-charge layers at the grain boundaries.

The formation of double Schottky depletion layers at the grain boundaries of ceramic $BaTiO_3$ and their impact on the properties of $BaTiO_3$ ceramics was first proposed by Heywang[13] in order to explain the unique positive temperature coefficient of resistance (PTCR) behavior around the Curie temperature, which only existed in donor-doped semiconducting $BaTiO_3$ ceramics. This model indicates that the depletion barriers are formed because of the electron trapping by acceptor states at grain boundaries. Jonker[14-15] later extended the Heywang model, considering the influence of ferroelectric polarization on resistivity below the Curie temperature.

In $BaTiO_3$-based MLCCs, the depletion layers are believed not only to be depleted of electron carriers and therefore to be highly resistive, but also to act as electrical barriers against oxygen vacancy electromigration and thus to slow down the degradation process.[2, 10, 16] Although high-resistance depletion layers both at grain boundaries and at electrode interfaces limit electronic conduction and the transport of oxygen vacancies across dielectric layers, oxygen vacancy migration is either trapped near the grain boundary depletion layers or blocked by electrode interfaces, and these charged oxygen vacancies are neutralized by the reduction of Ti^{4+} near the cathode and the rare-earth doping in the $BaTiO_3$ dielectric. This agrees with a number of recently published works about first-principles calculations of rare-earth element doping, the local atomic configuration, and the solution energy of oxygen vacancies.[17-19]

In this paper, the IR degradation in Ni-$BaTiO_3$ MLCCs was investigated for three commercial BME capacitors qualified to the same reliability level but made by different manufacturers. The paper provides insight into the time-dependent correlations among oxygen vacancy migration,

vacancy trapping, and the depletion layer height. A theoretical model based on the oxygen vacancy migration and entrapment at grain boundary is proposed to show the relationship between the reliability, characterized by MTTF, and the depletion layer height reduction during the IR degradation in the $BaTiO_3$ dielectric materials of BME capacitors.

II. EXPERIMENTAL PROCEDURE

Three automotive-grade commercial BME capacitors, AA47450, AB47450, and AC47450, with the same chip size, capacitance, and rated voltage, but made by different manufacturers, were selected for this study. These BME capacitors were qualified per AEC-Q200, a specification document developed by the Automotive Electronics Council of United States for ceramic capacitors and passive components used in harsh automotive environments. The microstructures of the three BME capacitor lots were investigated by cross-section processing of five (5) units per capacitor type and were examined using a scanning electron microscope (SEM) to reveal the number of dielectric layers, average grain size, and average dielectric layer thickness.

Table I summarizes the specifications, number of dielectric layers, corresponding electrical field (V/thickness), and volts per grain at a given stress condition used to degrade the capacitors to reveal their failure modes. The electric field can be calculated by dividing the measured dielectric thickness by the applied voltage. The volts per grain (the voltage applied to each individual $BaTiO_3$ grain) can be calculated by using the dielectric thickness and measured average grain size data from the microstructure analysis.

The results in Table I show that at a given applied voltage, the values of volts per grain are very similar among the three BME capacitor lots, indicating that these capacitors are not only manufactured and qualified to the same reliability level, but they will also have a similar applied electrical strength during degradation. The three BME capacitor lots were degraded together under the same HALT temperature and applied voltage conditions, as shown in Table I. Twenty (20) BME capacitors were tested for each stress condition and for each capacitor type.

Deliverable to NASA Electronic Parts and Packaging (NEPP) Program to be published on nepp.nasa.gov, paper published in the IEEE Transactions on Components, Packaging and Manufacturing Technology, Vol. 5, No. 1, January 2015.

Table I. Specifications and Calculated *E* (kV/mm), and Volts per Grain (V/Grain)

Part ID	Stress Level	E (kV/mm)	V/Grain
AA46450 0.47µF, 50V, 0805 Manufacturer A 98 layers $BaTiO_3$ thickness= 6.39 µm Ave. grain size= 0.38 µm	250V 175C	39.1236	14.75
	225V 165C	35.2113	13.27
	250V 165C	39.1236	14.75
	250V 155C	39.1236	14.75
	315V 155C	49.2958	18.59
AB47450 0.47µF, 50V, 0805 Manufacturer B 100 layers $BaTiO_3$ thickness= 5.80 µm Ave. grain size= 0.33 µm	250V 175C	43.0886	14.13
	225V 165C	38.7797	12.72
	250V 165C	43.0886	14.13
	250V 155C	43.0886	14.13
	315V 155C	54.2916	17.81
AC47450 0.47µF, 50V, 0805 Manufacturer C 103 layers $BaTiO_3$ thickness= 8.10 µm Ave. grain size= 0.40 µm	250V 175C	30.8642	12.45
	225V 165C	27.7778	11.20
	250V 165C	30.8642	12.45
	250V 155C	30.8642	12.45
	315V 155C	38.8889	15.68

The traditional HALT measures only the time-to-failure (TTF) data of each capacitor at a given stress condition and then uses a statistical model to determine the mean-time-to-failure (MTTF) data at this stress condition.[19-22] This approach is based on a single failure mode assumption and is adequate for most ceramic capacitors with precious-metal electrodes (PMEs). However, as has been previously shown, [26-29] many BME capacitors, when degraded under HALT conditions, reveal a more complicated failure mechanism with two distinct failure modes. A recently performed failure analysis of these degraded BME capacitors also confirms the existence of two distinct failure modes. [37] For this reason, the measurement of TTF data alone will not result in an accurate prediction of the reliability life of these BME capacitors. In order to characterize the multiple failure modes in BME capacitors, the leakage current was also monitored in-situ and was measured every 1-3 seconds for each capacitor unit. The reliability life of a capacitor is thus not only determined by the TTF data, but also by the measured leakage current data used to distinguish the failure modes. To differentiate this new approach from the traditional single-failure mode HALT that measures TTF data only, this modified method that has been used with multiple failure modes has been dubbed HALST, which stands for "highly accelerated life stress testing." [29] The term "HALST" is used through the remainder of this paper as appropriate.

When IR degradation is accelerated under HALST conditions, a certain value of IR or of leakage current must be used as the failure criterion at which the TTF can be determined. Per MIL-PRF-123, $BaTiO_3$-based MLCCs built for high-reliability applications were constructed with a minimum dielectric thickness of 25μm for rated voltages greater than 50V. In this case, the leakage current level was very low, even under HALST conditions. The MLCC was considered a failure when IR at a given stress condition was degraded three to four orders below its initial value.[20-21] Waser et al. have also defined characteristic lifetime t_{ch} at which the leakage current has risen one decade above its minimum value to evaluate the degradation rate.[10] With the progress in Ni-$BaTiO_3$ MLCC development, dielectric thicknesses have been significantly reduced, even below two microns.[22] As a result, leakage current has increased significantly, and Ni-$BaTiO_3$ MLCCs are considered to have failed at a fairly low IR value. Some reports define the TTF as the time at which IR is degraded to a value of 500kΩ,[22-23] 1,000kΩ,[24] or 10% of its initial value,[4] while others set a constant leakage current limit at 100μA for all of the stress conditions being used.[25-29] After a review of most of the failure criteria that have been reported for determining the TTF of MLCCs with $BaTiO_3$ dielectrics, the author of this study decided to use a single current limit of 100μA to determine the TTF for all stress levels and for all MLCC samples, based on the following considerations:

During HALST, each MLCC unit was connected in series to a current-limiting resistor with a DC power supply. The voltage drop across the series resistor was measured and used to calculate the leakage current of the capacitor. Since the voltage drop on the current-limiting resistor is dependent on the current value, a leakage current higher than 100μA can result in a voltage drop on the current-limiting resistor of more than 5% of the overall applied voltage. This is true for a number of BME capacitors with thin dielectric layers that can be degraded under fairly low applied voltages. Although this voltage drop can be reduced if a smaller-value resistor is used, the voltage value reading on a small resistor may be too low to ensure the accuracy of the IR measurement. For example, when an MLCC with a 100kΩ resistor is accelerated at 150V, the voltage drop will be 100kΩ·100μA = 10V, which is 6.7% of the total applied voltage. For a 1kΩ resistor, the voltage drop is only 0.1V across the resistor, which may be too low to show the details of the leakage current changing with the stress time. In this study, the values of the resistor were chosen such

that the maximum voltage drop at the current-limiting resistor will be no more than 3% of the applied voltage under all HALST conditions.

III. RESULTS AND DISCUSSION

A. Characterization of time-dependent leakage current and MTTF data

(1) Leakage current and MTTF data

FIG. 1 shows the leakage current against stress time for the three BME capacitor lots at a given stress condition: 155°C, 250V (5X rated voltage). The plots in FIG. 1 have the same scale on the x-axis. It can be seen that these capacitor lots, when degraded at the same stress condition, revealed significantly different TTF data. Further details about the characterization of the failure patterns and about the method to determine the acceleration factors have been discussed in a previous work.[29]

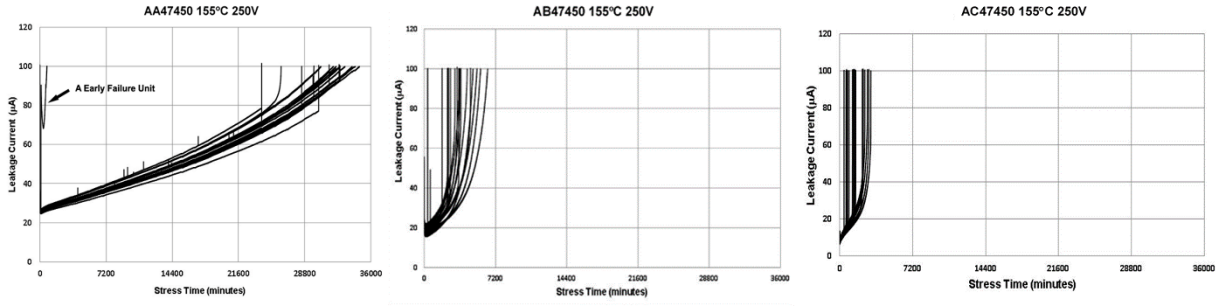

FIG. 1. Leakage current as a function of stress time for the three BME capacitor lots, degraded at 155°C, 250V. The plots were made with the same x-axis scale to reveal the difference in time-to-failure data.

A 2-parameter Weibull plot can be made when TTF data at a given stress level are available. The MTTF, a statistical parameter that measures reliability, can be determined as:

$$MTTF = \eta\Gamma(1 + \beta^{-1}), \quad (1)$$

where slope β is the dimensionless shape parameter whose value is often characteristic of the particular failure mode, η is the scale parameter that represents the time at which 63.2% of the population has failed, and $\Gamma(x)$ is the gamma function of x.

Table II summarizes the calculated MTTF data using Eq. (1) when all TTF data at a given stress level were used to make a 2-parameter Weibull plot. The reliability life, as characterized by MTTF, was more than one magnitude of difference among the capacitor lots under the same stress condition.

Table II. Mean-Time-to-Failure Data of the Three BME Capacitor Lots at Various Stress Conditions

	MTTF (Minutes) of BME Capacitors		
Test Conditions	AA47450	AB47450	AC47450
250V 175C	1466	450	319
250V 165C	9869	1140	626
225V 165C	15423	2066	1046
250V 155C	31602	3659	1479
250V, 145C	86400	8895	2458
315V 155C	17721	1102	648

(2) Characterization of leakage current data for a slow degradation failure mode

As shown in Table I, all three BME capacitor lots that were made for the same reliability level revealed almost identical construction and microstructure parameters and were also degraded under very similar stress conditions. However, the MTTF data contained in Table II show significant differences in reliability life for these BME capacitors. In order to understand the mechanism that determines the reliability life, the leakage current data shown in FIG. 1 were re-plotted with a different scale in the x-axis to reveal details of the differences in their failure modes. As shown in FIG. 2, the TTF data appear to be highly dependent on the failure mode exhibited during the HALST regimen.

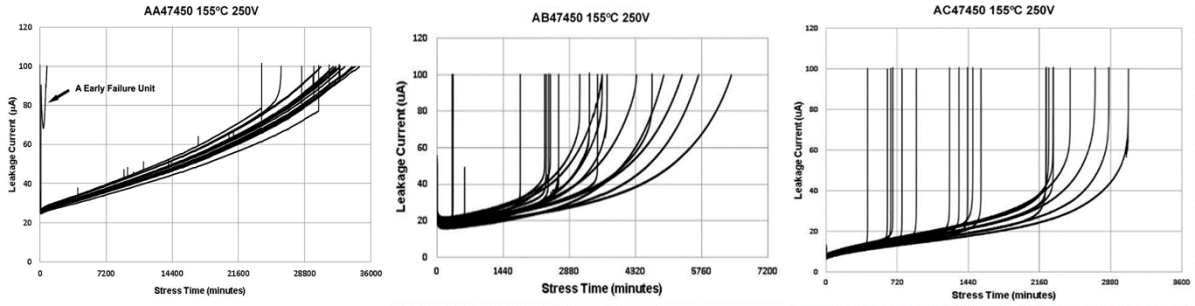

FIG. 2. Leakage data are re-plotted from FIG. 1 with a different scale in the x-axis to reveal details in the failure modes among the three BME capacitor lots.

As discussed in previous works,[27-29] two failure modes can be identified in these BME capacitor lots: catastrophic and slow degradation. A catastrophic failure is characterized by a time-accelerating increase in leakage current that is mainly due to existing processing defects (voids, cracks, delaminations, etc.) or to extrinsic defects. A slow degradation failure is characterized by a near-linear increase in leakage current against stress time; this is caused by the electromigration

of oxygen vacancies (intrinsic defects). The TTF data shown in FIG. 2 clearly indicate that BME capacitors with slow degradation failures exhibit the largest MTTF values (AA47450), and those with the most catastrophic failures showed the smallest MTTF values (AC47450). Capacitor lot AB47450 shows failures with both failure modes and with MTTF values in between those of the other two capacitor lots.

As shown in FIG. 2, for a certain period of stress time, the leakage current follows a slow degradation failure mode, i.e., a gradual increase in leakage current against stress time. With a further increase of stress time, some capacitors will fail catastrophically, while some will retain the slow degradation failure mode until the failure criterion is reached.

The leakage data shown in FIG. 2 have been curved-fitted with a number of different mathematical functions (power law, exponential, linear, logarithmic, etc.). Although the leakage data shown in FIG. 2 appear to be linear against most of the stress time measured, the curve-fitting results have shown that the exponential form of

$$I = I(t_0)e^{\left(\frac{t-t_0}{\tau_{SD}}\right)} \tag{2}$$

fits the leakage data better than a linear form. In Eq. (2), I is the measured leakage current, $I(t_0)$ is the leakage value at $t=t_0$, and τ_{SD} is a characteristic exponential growth time.

FIG. 3 shows an example of curve fitting using Eq. (2) for two capacitor samples with different failure modes. C13, with a near-linear increase in leakage, fits very well to Eq. (2) when all of the measured leakage data points and a method of least squares were used. Although C7 fails with a catastrophic failure characterized by a rapid leakage current increase at the end, the majority of the leakage data follow a slow degradation failure mode and still fit well to Eq. (2). A similar value of τ_{SD} to that of C13 could be obtained. For some of the leakage data that finished with a strong catastrophic failure, in order to obtain a proper value of τ_{SD}, some of the leakage data points at the catastrophic failure side have to be gradually removed until a value of $R^2 \geq 0.99$ is reached.

The meaning of τ_{SD} can be illustrated by the following example: Let I_1 and I_2 be the leakages at t_1 and t_2, respectively, for a slow degradation failure. If one assumes $\frac{I_2}{I_1} = 2$, then Eq. (2) can be rewritten as:

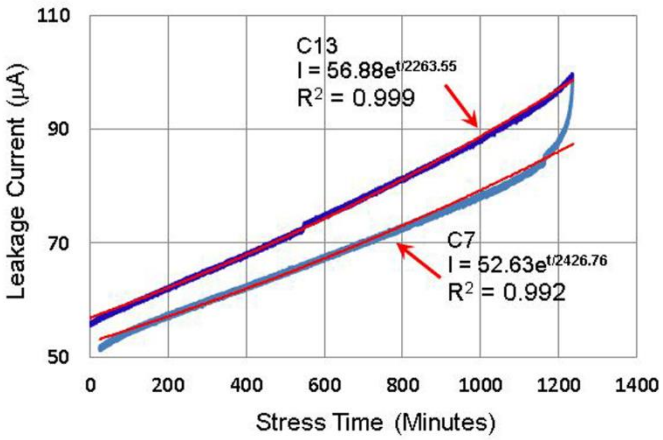

FIG. 3. Examples of curve fitting using Eq. (2) for two BME capacitor samples with different failure patterns. Both appear to fit well to the exponential form of Eq. (2) for most of the stress time.

$$\frac{I_2}{I_1} = e^{\left(\frac{t_2 - t_1}{\tau_{SD}}\right)} = e^{\left(\frac{\Delta t}{\tau_{SD}}\right)} = 2$$

and

$$\tau_{SD} = \frac{\Delta t}{ln(2)} \approx 1.4427 \cdot \Delta t, \quad (3)$$

where Δt is the time at which the leakage current doubles in value. The greater the value of τ_{SD}, the longer the timespan of a degradation failure, indicating a slower IR degradation process.

At a given stress condition, when the τ_{SD} of all 20 BME capacitors being tested was obtained using the curve-fitting method described above, a 2-parameter Weibull plot could be made, and an average value of τ_{SD}, $<\tau_{SD}>$, was defined as the scale parameter η of the Weibull plot.

Table III summarizes the values of $<\tau_{SD}>$ determined for various stress conditions. The table can be used to compare the corresponding MTTF data. In most cases, the value of $<\tau_{SD}>$ was greater than that of MTTF, but it was smaller in a few lower-stress levels where the catastrophic failure mode is dominant. Certainly the relationship between TTF and τ_{SD} depends upon the failure criterion, and if a fixed absolute value of leakage current is selected as the failure criterion, then the relationship depends on the value chosen and on the initial leakage current value for the capacitors.

Table III. Calculated MTTF Data from Weibull Plots of TTF Data and Calculated $<\tau_{SD}>$ from the Curve-fitting of the Three BME Capacitor Lots at Three Degradation Conditions

	MTTF (Minutes)	$<\tau_{SD}>$ (Minutes)
Test Conditions	AA47450	
250V, 175°C	1466	3333
250V, 165°C	9869	11111
250V, 155°C	31602	34925
Test Conditions	AB47450	
250V, 175°C	450	667
250V, 165°C	1140	1714
250V, 155°C	3659	3333
Test Conditions	AC47450	
250V, 175°C	319	357
250V, 165°C	626	769
250V, 155°C	1479	1667

B. An IR degradation model for BME capacitors

(1) Time-dependent depletion layer height $\phi(t)$

Although the formation of a double Schottky barrier layer at a grain boundary as shown in FIG. 4 was initially proposed to explain the PTCR effect in donor-doped semiconducting $BaTiO_3$ ceramics,[13-15] the same barrier depletion layer model has also been suggested to explain the IR degradation in Ni-$BaTiO_3$ MLCCs.[2, 4, 9-11] The typical barrier height can be expressed as

$$\phi = \frac{e^2 N_d d^2}{2\varepsilon_0 \varepsilon_r},$$

where N_d is the donor concentration, d is the depletion layer thickness, e is the electron charge, and $\varepsilon_0\varepsilon_r$ is the dielectric constant. The electro-neutrality condition in the depletion layer satisfies the following requirement:[13]

$$d = \frac{n_s}{2N_d}, \tag{4}$$

where n_s is the concentration of *trapped electrons* at grain boundary surface acceptor states (the number is N_s) (cm^{-2}). The barrier height ϕ can be rewritten as

$$\phi = \frac{e^2 n_s^2}{8\varepsilon_0 \varepsilon_r N_d}. \tag{5}$$

Eq. (5) has often been used to estimate the grain boundary barrier height in semiconducting $BaTiO_3$ ceramics.[34, 38] In Ni-$BaTiO_3$ MLCCs, N_d is mainly determined by the bulk concentration of ionized oxygen vacancies. Although oxygen vacancies migrate under an applied DC field and the weakly bonded electrons can be trapped by the surface acceptor states, the value of depletion layer thickness d in Eq. (4) is always in the submicron range, indicating that $N_d >> n_s$. Therefore, one can assume that $N_d(t) \approx N_d(0)$, and one can also assume time independence. Therefore, the time-dependent barrier height ϕ can be expressed as

$$\frac{d\phi(t)}{dt} = \frac{d}{dt}\left(\frac{e^2 n_s^2}{8\varepsilon_0 \varepsilon_r N_d}\right) = \frac{e^2}{4\varepsilon_0 \varepsilon_r N_d}\frac{dn_s(t)}{dt}.$$

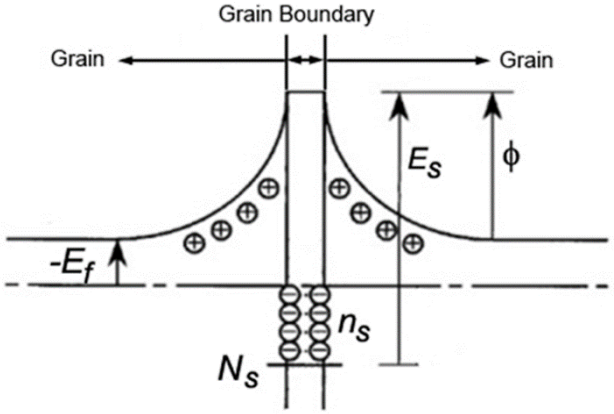

FIG. 4. Schematic illustration of the formation of a double Schottky barrier around the grain boundary of a $BaTiO_3$ ceramic capacitor, where ϕ is the depletion barrier height; n_s is the concentration of *trapped electrons* at the grain boundary surface acceptor states whose number is N_s (cm^{-2}); and E_s is the energy level of the surface states from the conduction level of the bulk.

In order to determine $\frac{dn_s(t)}{dt}$, the following facts were considered: 1) $n_s(t)$ is trapped electrons at surface acceptor states in the grain boundary regions. The negative space charge due to trapped electrons is compensated for by the formation of a positive space charge region near the grain boundary, which behaves like a depletion barrier layer to electron conduction. 2) The computational analysis on the trapping of oxygen vacancies at grain boundaries with respect to local atomic configuration and energy shows that grain boundaries attract oxygen vacancies and trap them at specific sites at which local cation density is lower than that in the grain interior.[17] 3) Since oxygen vacancies behave like donors, they possess positive space charges when ionized.

The same positive space charge in a barrier layer at a grain boundary will thus act as a resistance for positively charged oxygen vacancy diffusion in a polycrystalline $BaTiO_3$ dielectric. As a result, when an ionized oxygen vacancy migrates under a DC field and reaches the barrier layer, it has a tendency to become trapped there. The electro-neutrality condition requires that the weakly bonded two electrons that are moving in a conduction band now have to be localized in order to make the trapped oxygen vacancy neutralize and to become part of the crystalline structure. When Kroger and Vink symbols are used,[31] the process can be described by

$$V_O = V_O^{\bullet\bullet} + 2e'. \tag{6}$$

As previously reported,[4] the localized electrons that compensate the $V_O^{\bullet\bullet}$ localization can be trapped with the reduction of *Ti* ions surrounding the $V_O^{\bullet\bullet}$ as $Ti^{4+} + e' \rightarrow Ti^{3+}$, and $Ti^{3+} + e' \rightarrow Ti^{2+}$.[4] The reduction of Ti^{4+} will now reduce the positive space charge in the positively charged depletion layer and reduce the barrier height. Since the barrier height is balanced by the trapped electrons in surface acceptor states $n_s(t)$, the reduction in barrier height will lower the Fermi level at grain boundary and then will reduce the $n_s(t)$. If we assume that Δn_O is the electron concentration that has been localized to make the trapped $V_O^{\bullet\bullet}$ neutral, Δn_O should meet the following conditions: at $t = 0$, $\Delta n_O(0) = 0$, and at $t \rightarrow \infty$, $\Delta n_O = n_s(0)$, i.e., all trapped electrons at $t = 0$ in the surface acceptor states $n_s(0)$ will eventually be fully compensated for by the localized electrons that neutralize the trapped $V_O^{\bullet\bullet}$. However, with a further increase of Δn_O as more $V_O^{\bullet\bullet}$ are trapped and neutralized, the electrically negative feature of $n_s(t)$ will further retard the localization of electrons and reduce the localization rate of Δn_O. Therefore, the change of Δn_O as a function of *t* can be expressed by a first-order reaction according to the reaction rate theory[30]

$$\frac{d\Delta n_O(t)}{dt} = K(t)[n_s(0) - \Delta n_O(t)],$$

and

$$\int_{\Delta n_O(0)}^{\Delta n_O(t)} \frac{d\Delta n_O(t)}{\Delta n_O(t) - n_s(0)} = \int_0^t -K(t)dt \tag{7}$$

where *K(t)* is the degradation rate constant and $n_s(0) - \Delta n_O(t) = n_s(t)$ is the trapped electron concentration at surface acceptor states at time *t*. If $\Delta n_O(t)$ is only balanced by $n_s(t)$ near the

Fermi level, $K(t) = K = K_0 e^{-\frac{E_k}{kT}}$ can be simplified as a time-independent constant in which E_k is the activation energy that is required for $V_O^{\bullet\bullet}$ in electromigration to be neutralized at a grain boundary region per Eq. (6) and *k* is the Boltzmann constant. Since $\Delta n_O(0) = 0$, Eq. (7) finally yields

$$\frac{n_s(0) - \Delta n_O(t)}{n_s(0)} = e^{-\mathrm{K}t},$$

and

$$\Delta n_O(t) = n_s(0)(1 - e^{-\mathrm{K}t}), \tag{8}$$

the remaining trapped electrons in acceptor states can be simply expressed according to Eq. (8) as

$$n_s(0) - \Delta n_O(t) = n_s(0) - n_s(0)(1 - e^{-\mathrm{K}t}) = n_s(0)e^{-\mathrm{K}t}.$$

Combining Eqs. (5) and (8) yields a time-dependent barrier height

$$\phi(t) = \frac{e^2[n_s(0) - \Delta n_O(t)]^2}{8\varepsilon_0 \varepsilon_r N_d} = \phi(0)\mathrm{e}^{-2\mathrm{K}t}. \tag{9}$$

This relationship indicates that the barrier height will exponentially decrease with time due to the oxygen vacancy entrapment at grain boundaries.

(2) Determination of degradation rate constant *K*

The measurement of *I-V* characteristics of ceramic $BaTiO_3$ inside the grain interior and at the grain boundary has shown that under an applied field of 100kV/cm, the current density inside the grain and at the grain boundary can differ by several orders of magnitude. The difference increases significantly as temperature increases. [33] It is the grain boundary that holds the high resistivity of the ceramic $BaTiO_3$. If all grain boundaries inside a dielectric layer are assumed to have a uniform barrier height $\phi(t)$, the time-dependent resistivity $\rho(t)$ of an MLCC can be written as[13]

$$\rho(t) = \rho_0 e^{\left(\frac{\phi(t)}{kT}\right)}, \tag{10}$$

where ρ_0 is the resistivity of the grain interier. According to Eq. (2), the time-dependent current density of an MLCC $j(t)$ for a slow degradation failure mode can be expressed as

$$j(t) = j(t_0)e^{\left(\frac{t-t_0}{\tau_{SD}}\right)} = \frac{E}{\rho(t)},$$

or

$$\rho(t) = \frac{E}{j(t_0)}e^{-\left(\frac{t-t_0}{\tau_{SD}}\right)}, \tag{11}$$

where $j(t_0)$ is the current density at $t = t_0$ and E is the applied field. Combining Eqs. (10) and (11) results in

$$\rho(t) = \rho_0 exp\left(\frac{\phi(t)}{kT}\right) = \rho_0 exp\left(\frac{\phi(0)\mathrm{e}^{-2\mathrm{Kt}}}{kT}\right) = \frac{E}{j(0)} exp\left(-\frac{t-t_0}{\tau_{SD}}\right).$$

At a given stress level, E is a constant, so

$$\frac{t-t_0}{\tau_{SD}} \approx -\frac{\phi(0)}{kT}\mathrm{e}^{-2\mathrm{Kt}}. \tag{12}$$

Using $\langle\tau_{SD}\rangle$, the average of τ_{SD}, to replace τ_{SD}, and $e^{-x} \approx 1 - x$ when x is small, the integration of Eq. (12) results in

$$\int_0^{MTTF} \frac{t-t_0}{\langle\tau_{SD}\rangle} dt = -\int_0^{MTTF} \frac{\phi(0)}{kT} \cdot \mathrm{e}^{-2\mathrm{Kt}} dt \approx -\int_0^{MTTF} \frac{\phi(0)}{kT}(1-2Kt)dt,$$

and

$$\frac{1}{2\langle\tau_{SD}\rangle} \approx \frac{\phi(0)}{kT}\left(K - \frac{1}{MTTF}\right).$$

This gives rise to

$$\frac{1}{MTTF} = K - \frac{kT}{2\phi(0)\langle\tau_{SD}\rangle} \approx K_0 e^{-\frac{E_k}{kT}}. \tag{13}$$

Eq. (13) is the well-known Prokopowicz-Vaskas equation for MLCCs, when applied voltage is a constant.[35] The degradation rate constant K can now be determined by an Arrhenius plot using the MTTF data obtained at various temperatures and at a constant voltage.

Using the MTTF data at different temperatures and at a given voltage (250V) for the three BME capacitor lots, a corresponding Arrhenius plot according to Eq. (13) can be plotted, as shown in FIG. 5. Both activation energy E_k and degradation rate constant K_0 can now be determined.

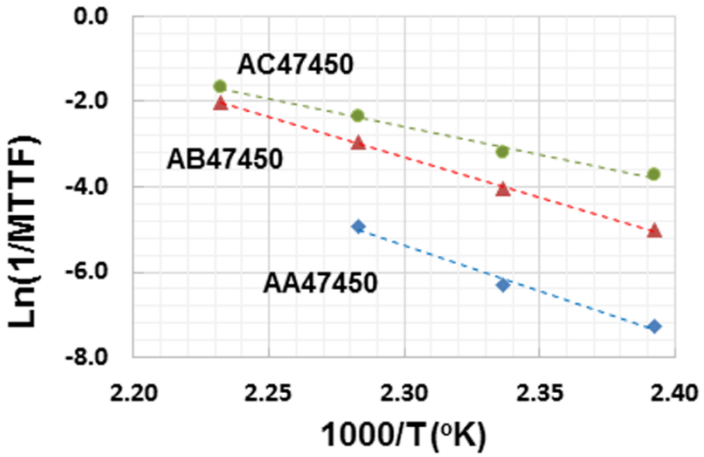

FIG. 5. Arrhenius plots using Eq. (13) and measured MTTF data in Table II for the three BME capacitor lots.

Table IV lists the activation energy E_k and constant K_0 at three different temperatures for the three BME capacitor lots. The calculated *K* values shown in Table IV were used to estimate the MTTF data per Eq. (13). A comparison between the measured MTTF data and the calculated data shows fairly good agreement. All calculated MTTF values are smaller than the measured ones. For lot AA47450, the MTTF data measured at 175˚C were excluded for the estimation of the degradation rate constant *K* because its value is much smaller when combined with other MTTF data points to give rise to a good linear fitting. Since the BME capacitor lot under degradation was so leaky at this temperature, the results of self-heating due to the leakage current could result in a significant amount of temperature increase and thus an acceleration in the failure of the BME capacitors.

Table IV. Calculated Degradation Constant *K* and MTTF Data per the Curve-Fitting Results in FIG. 5 and Eq. (13)

	$K_0 e^{\frac{-E_k}{kT}}(hour^{-1})$			MTTF (minutes) at 155°C, 250V	
Capacitor ID	E_k (eV)	at 398K (125°C)	at 428K (155°C)	Measured	Calculated
AA47450	1.65	7.38×10^{-5}	2.10×10^{-3}	31602	28640
AB47450	1.63	6.76×10^{-4}	1.86×10^{-2}	3459	3218
AC47450	1.11	4.94×10^{-3}	4.73×10^{-2}	1479	1268

Deliverable to NASA Electronic Parts and Packaging (NEPP) Program to be published on nepp.nasa.gov, paper published in the IEEE Transactions on Components, Packaging and Manufacturing Technology, Vol. 5, No. 1, January 2015.

C. IR degradation mechanism due to oxygen vacancy electromigration

(1) Reliability and oxygen vacancy migration

According to Eq. (9),

$$\phi(t) = \phi(0)\mathrm{e}^{-2\mathrm{Kt}} = \phi(0)\mathrm{e}^{-\frac{2\mathrm{t}}{MTTF}},$$

and

$$\frac{1}{MTTF} = \approx K_0 e^{-\frac{E_k}{kT}},$$

where $K = K_0 e^{\frac{-E_k}{kT}}$ is the degradation rate constant for oxygen vacancy entrapment at grain boundaries. Although *K* and MTTF can be related to each other per the Prokopowicz-Vaskas equation, the physical meaning of *K* was clearly defined in the proposed model. To make Ni-$BaTiO_3$ BME capacitors with improved reliability, the value of *K* must be minimized. This requires a smaller value of the degradation constant K_0, which is the total number of oxygen vacancies that are migrate-able; and a large value of E_k, which is the activation energy required for $V_O^{\bullet\bullet}$ to be neutralized and trapped near the depletion layer at grain boundaries. This has been proven from the calculated *K* values shown in Table IV, where AA47450 and AB47450 are shown to have similar values of E_k but a much smaller value for K_0, which gives rise to a significantly improved reliability life (larger MTTF) for capacitor AA47450.

On the other hand, since a typical barrier height value of $\phi(0) \approx$1.30eV has been reported previously,[4] a large value of $E_k > \phi(0)$ is necessary to slow down the $V_O^{\bullet\bullet}$ entrapment, because a large value of E_k also means that the entrapment of $V_O^{\bullet\bullet}$ at grain boundaries may not be an energetically favorable process unless the barrier height $\phi(t)$ is high enough to be comparable to E_k. This is the case for AC47450, where E_k=1.11eV is smaller than that of $\phi(0)$. Therefore, the oxygen vacancies are more energetically favorable for local entrapment than for migrating across the depletion barrier, and they result in a very small reliability life when compared to the other two BME capacitor lots.

Finally, since $N_d \gg n_s$ per Eq. (4), only a tiny fraction of oxygen vacancies can be trapped at the grain boundaries during the electromigration across the dielectric layer to cause IR degradation.

This indicates that the effort to simply reduce the level of $V_O^{\bullet\bullet}$ in the dielectric material would not significantly slow down the IR degradation. Indeed, a small value of K_0 indicates that the number of electromigrate-able $V_O^{\bullet\bullet}$ must be minimized. The recent first-principles calculations based on the density function theory have shown that some kinds of dopants in $BaTiO_3$ dielectrics, such as rare-earth (RE) and alkaline-earth (AE) elements, were effective in improving the reliability life of Ni-$BaTiO_3$ capacitors.[17-19] According to the IR degradation model proposed here, both RE and AE doping would benefit from the "frozen" migrate-able $V_O^{\bullet\bullet}$ and thus reduce the value of K_0. On the other hand, some RE doping elements, such as Dy and Er, due to their "amphoteric" characteristics, will also benefit from the formation of deep surface acceptable states N_S to result in a large value of E_k. The correlations between the formulation and the value of the degradation rate constant for oxygen vacancy entrapment K as defined in this work needs to be further investigated.

(2) Insulation resistance and reliability life

According to Eq. (12),

$$e^{\frac{t-t_0}{\tau_{SD}}} \approx e^{-\frac{\phi(0)}{kT}\mathrm{e}^{-2\mathrm{Kt}}},$$

which indicates that a slower IR degradation process, characterized by a larger value of τ_{SD}, would give rise to a smaller value of $\phi(0)$. This makes sense since a smaller $\phi(0)$ will energetically be favorable to the continuous electromigration of $V_O^{\bullet\bullet}$ without being trapped at a grain boundary to cause an IR degradation. However, this is only one part of the equation; $\phi(0)$ also presents the barrier height for the conduction band electronic carriers. A lower $\phi(0)$ will facilitate electronic conduction and will also deteriorate the IR. As a result, when electron conduction and oxygen vacancy electromigration are both taken into account, a moderate initial barrier height $\phi(0)$ and a smaller K are the keys for slowing the IR degradation in Ni-$BaTiO_3$-based ceramic capacitors and thus improving their reliability life.

As an important conclusion of this model development, higher IR values may not always result in a larger MTTF, but a slower IR degradation rate (smaller K) will always have this effect. This conclusion can be verified from the measured leakage data shown in FIG. 3, where sample

AC47450 was shown to have the highest initial IR values and smallest MTTF and AA47450 had the lowest initial IR values but the largest MTTF among the group.

A higher $\phi(0)$ generally means a higher resistance and therefore a higher electrical strength when a DC voltage is applied. A higher DC electrical strength makes it more likely that a "thermal-related electrical breakdown" will be experienced due to the localization of the electrical strength.[9-11]

(3) Oxygen vacancy migration and compensation

Since only a very small portion of $V_O^{\bullet\bullet}$ may be trapped at the grain boundaries, the majority of $V_O^{\bullet\bullet}$ will continually migrate and will eventually reach the dielectric layer and internal Ni electrode interface, as has been shown by previously reported electron energy loss spectroscopy (EELS) and high-resolution transmission electron microscope (HRTEM) observations.[4]

Since there is no evidence to show that $V_O^{\bullet\bullet}$ can be transferred across the cathode electrode layer,[4,10] most $V_O^{\bullet\bullet}$ capable of migration will now pile up along the Ni-electrode dielectric interface. To neutralize these vacancies, a significant number of electrons is required, which can only be obtained from the cathode electron injection. The energy required for cathode electron injection at the dielectric-electrode interface is ~1.25eV.[36] If E_k is less than this, most of the oxygen vacancies will be energetically favorable for localization, and a quick IR degradation will occur. This is exactly the case for lot AC47450.

The high concentration of localized electrons due to the compensation of the pile-up of oxygen vacancies will not only dramatically change the local stoichiometry of the $BaTiO_3$ dielectric, but it will also lead to a leakage current increase during IR degradation. This will cause a local temperature increase and will eventually lead to the breakdown at the Ni-$BaTiO_3$ interface. The initial failure site of the dielectric-electrode interface was clearly revealed in a previously published failure analysis work regarding Ni-$BaTiO_3$ ceramic capacitors.[37]

IV. SUMMARY AND CONCLUSIONS

Three BME capacitor lots with the same specification (chip size, capacitance, and rated voltage) and reliability level, made by three different manufacturers, were selected for reliability performance evaluation. The microstructure analysis of these capacitors showed that the three

BME products had a similar number of dielectric layers and a similar number of grains per dielectric layer. When an external voltage was applied, the volts per grain was almost identical for these capacitors, indicating that the dielectrics will experience the same voltage stress when electrically tested under the same externally applied voltages.

These BME capacitors were then degraded using HALST under the same temperature and applied voltage conditions. The reliability life, as characterized by MTTF, differed by more than one order of magnitude among the capacitor lots.

A model based on the existence of depletion layers at grain boundaries and on the entrapment of electromigrate-able oxygen vacancies was proposed to explain the MTTF difference among these BME capacitors. The MTTF has been found to be directly related to the degradation rate constant *K* of oxygen vacancy entrapment at grain boundaries. The MTTF and *K* were found to follow the traditional Prokopowicz-Vaskas equation at a constant applied voltage.

A lower depletion layer height $\phi(0)$ is energetically favorable for a slower degradation rate and a longer reliability life. However, when both oxygen vacancy migration and electronic conduction are taken into account, a $\phi(0)$ with a moderate height would give rise to the best reliability performance.

It is the conclusion of this study that reliability will not be improved simply by increasing the insulation resistance. Indeed, Ni-$BaTiO_3$ BME capacitors with a smaller IR degradation rate constant *K*, or a smaller amount of entrapped $V_O^{\bullet\bullet}$ at grain boundaries, will always give rise to a longer reliability life.

Both RE and AE doping may have profound impacts on the values of degradation rate constant *K*, and the impacts needs to be further investigated.

Acknowledgements

The author appreciates the NASA Electronic Parts and Packaging (NEPP) program's support for this study. The author would like to thank the NASA Goddard Space Flight Center Code 562 Parts Analysis Laboratory for assistance with electrical testing.

References:

[1] H. Kishi, Y. Mizuno, and H. Chazono, "Base-Metal Electrode-Multilayer Ceramic Capacitors: Past, Present and Future Perspectives." Jpn. J. Appl. Phys., Part 1, vol. 42 no. 3, pp. 1-15, January 2003.

[2] H. Chazono and H. Kishi, "dc-Electrical Degradation of the BT-Based Material for Multilayer Ceramic Capacitor with Ni internal Electrode: Impedance Analysis and Microstructure." Jpn. J. Appl. Phys., Part 1, vol. 40, no. 9B, pp. 5624–5629, September 2001.

[3] G. Y. Yang, G. D. Lian, E. C. Dickey, C. A. Randall, D. E. Barber, P. Pinceloup, M. A. Henderson, R. A. Hill, J. J. Beeson, and D. J. Skamser, "Oxygen Nonstoichiometry and Dielectric Evolution of BaTiO3. Part I—Improvement of Insulation Resistance with Reoxidation." J. Appl. Phys., Vol. 96, no. 12, pp. 2492-2499, December 2004.

[4] G. Y. Yang, G. D. Lian, E. C. Dickey, C. A. Randall, D. E. Barber, P. Pinceloup, M. A. Henderson, R. A. Hill, J. J. Beeson, and D. J. Skamser, "Oxygen Nonstoichiometry and Dielectric Evolution of BaTiO3. Part II—Insulation Resistance Degradation Under Applied DC Bias." J. Appl. Phys., Vol. 96, no. 12, pp. 7500-7508, December 2004.

[5] K. Morita, Y. Mizuno, H. Chazono, and H. Kishi, "Effect of Mn Addition on dc-Electrical Degradation of Multilayer Ceramic Capacitor with Ni Internal Electrode." Jpn. J. Appl. Phys., Part 1, vol. 41, no. 11, pp. 6957-6961, November 2002.

[6] H. Chazono and H. Kishi, "Effect of Ho Amount on Microstructure and Electrical Properties for Ni-MLCC." Key Eng. Mater., Vol. 2, no. 48, pp.183-186, August 2003.

[7] D. F. K. Hennings, "Dielectric Materials for Sintering in Reducing Atmospheres." J. Eur. Ceram. Soc., Vol. 21, no. 10-11, pp. 1637-1642, November 2001.

[8] Albertsen, K., Hennings, D. and D. Steigelmann, "Donor-Acceptor Charge Complex Formation in Barium Titanate Ceramics: Role of Firing Atmosphere." J. Electroceram., Vol. 2, no. 3, pp. 193-198, November 1998.

[9] R. Waser, "Electrochemical Boundary Conditions for Resistance Degradation of Doped Alkaline-Earth Titanates." J. Am. Ceram. Soc., Vol. 72, no. 12, pp. 2234-2240, December 1989.

[10] R. Waser, T. Baitu, and K.H. Härdtl, "dc Electrical Degradation of Perovskite-Type Titanates: I. Ceramics." J. Am. Ceram. Soc., Vol. 73, no. 6, pp. 1645-1653, June 1990.

[11] R. Waser, T. Baiatu, and K. H. Härdtl, "dc Electrical Degradation of Perovskite-Type Titanates: II. Single Crystals." J. Am. Ceram. Soc., Vol.73, no. 6, pp. 1654-1662, June 1990.

[12] T. Baiatu, R. Waser, and K. H. Härdtl, "dc Electrical Degradation of Perovskite-Type Titanates: III. A Model of the Mechanism." J. Am. Ceram. Soc., Vol. 73, no. 6, pp. 1663-1673, June 1990.

[13] W. Heywang, "Resistivity Anomaly in Doped Barium Titanate." J. Am. Ceram. Soc., Vol. 47, no. 10, pp. 484-490, October 1964.

[14] G. Jonker, "Some Aspects on Semiconducting Barium Titanate." Solid-State Electron., Vol. 7, pp. 895-903, July 1964.

[15] G. Jonker, "Halogen Treatment of Barium Titanate Semiconductors." Mat. Res. Bull., Vol. 2, no. 4, pp. 401–407, April 1967.

[16] M. Vollman and R. Waser, "Grain Boundary Defect Chemistry of Acceptor-Doped Titanates: Space Charge Layer Width." J. Am. Ceram. Soc., Vol. 77, no. 1, pp. 235-243, January 1994.

[17] T. Oyama, N. Wada, H. Takagi, and M. Yoshida, "Trapping of Oxygen Vacancy at Grain Boundary and its Correlation with Local Atomic Configuration and Resultant Excess Energy in Barium Titanate: A Systematic Computational Analysis." Phys. Rev. B, Vol. 82, no. 13, pp. 134107-134116, July 2010.

[18] A. Honda, S. Higai, Y. Motoyoshi, N. Wada, and H. Takagi, "Theoretical Study on Interactions Between Oxygen Vacancy and Doped Rare-Earth Elements in Barium Titanate." J. Appl. Phys., Vol. 50, no. 10, pp. 1143-1146, October 2011.

[19] H. Moriwake, C. A. J. Fisher, and A. Kuwabara, "First-Principles Calculations of Rare-Earth Dopants in $BaTiO_3$." J. Appl. Phys., Vol. 48, no. 9, pp. KC031-KC036, September 2009.

[20] W. Minford, "Accelerated Life Testing and Reliability of High K Multilayer Ceramic Capacitors." IEEE Transactions on Components, Hybrids, and Manufacturing Tech., Vol. 5, no. 3, pp. 297–300, September 1982.

[21] H. Pak and B. Rawal, "Reliability Prediction of Multilayer Ceramic Capacitors Using an Improved Accelerated Life Test and Weibull Analysis Technique." Proc. SPIE, Vol. 3235, pp. 362-367, October 1997.

[22] M. Randall, A. Gurav, D. Skamser, and J. Beeson, "Lifetime Modeling of Sub 2 Micron Dielectric Thickness BME MLCC." CARTS Proceedings, Scottsdale, AZ, pp. 134-141, March 2003.

[23] J. Yoon, K. Lee, and S. Lee, "Analysis of the Reliability of Multilayer Ceramic Capacitors with Inner Ni Electrodes Under Highly Accelerated Life Test Conditions." Tran. on Electrical and Electronic Mater., Vol. 10, no. 1, pp. 1229-1234, February 2009.

[24] M. Cozzolino, "A Comparison of BME and Traditional Technology Ceramic Capacitors." CARTS Proceedings, Orlando, FL, pp. 385-394, April 2006.

[25] T. Ashburn and D. Skamser, "Highly Accelerated Testing of Capacitors for Medical Applications." Proceedings of the 5th SMTA Medical Electronics Symposium, Anaheim, CA, pp.124-131, January 2008.

[26] J. Paulsen and E. Reed, "Highly Accelerated Lifetesting of Base-Metal-Electrode Ceramic Chip Capacitors." Microelectronics Reliability, Vol.42, no. 6, pp. 815-820, June 2002.

[27] D. Liu and M. Sampson, "Reliability Evaluation of Base-Metal-Electrode Multilayer Ceramic Capacitors for Potential Space Applications." CARTS Proceedings, Jacksonville, FL, pp. 45-63, March 2011.

[28] D. Liu and M. Sampson, "Some Aspects of the Failure Mechanisms in $BaTiO_3$-Based Multilayer Ceramic Capacitors." CARTS Proceedings, Las Vegas, NV, pp. 59-71, March 2012.

[29] D. Liu, "Highly Accelerated Life Stress Testing (HALST) of Base-Metal Electrode Multilayer Ceramic Capacitors." CARTS Proceedings, Houston, TX, pp. 235-248, March 2013.

[30] D. Viehland, S. Jang, L. E. Cross, and M. Wuttig, "Deviation from Curie-Weiss behavior in Relaxor Ferroelectrics." Phys. Rev. B, Vol. 46, no. 13, pp. 8003-8006, October 1992.

[31] F. Kröger and H. J. Vink, "Relations Between the Concentrations of Imperfections in Crystalline Solids." Solid-State Phys., Vol. 3, pp. 307–435, March 1956.

[32] K. Connors, *Chemical Kinetics, the Study of Reaction Rates in Solution*, VCH Publishers, New York, 1991.

[33] T. Nakamura, T. Yao, J. Ikeda, N. Kubodera, and H. Takagi. "Improvement of the Reliability of Dielectrics for MLCC." *IOP Conference Series: Materials Science and Engineering*, Vol. 18, no. 9, pp. 092007-092012, IOP Publishing, 2011.

[34] E. Brzozowski and M. Castro, "Influence of Nb^{5+} and Sb^{3+} Dopants on the Defect Profile, PTCR Effect and GBBL Characteristics of $BaTiO_3$ Ceramics." J. European Cer. Soc., Vol. 24, no. 8, pp. 2499–2507, July 2004.

[35] T. I. Prokopowicz and A. R. Vaskas, "Research and Development, Intrinsic Reliability, Subminiature Ceramic Capacitors." Final Report ECOM-90705-F, NTIS AD-864068, October 1969.

[36] A. Polotai, I. Fujii, D. Shay, G. Yang, E. Dickey, and C. Randall, "Effect of Heating Rates During Sintering on the Electrical Properties of Ultra-Thin Ni–$BaTiO_3$ Multilayer Ceramic Capacitors." J. Am. Ceram. Soc., Vol. 91, no. 8, pp. 2540-2544, August 2008.

[37] R. Weachock and D. Liu, "Failure Analysis of Dielectric Breakdowns in Base-Metal Electrode Multilayer Ceramic Capacitors." CARTS Proceedings, Houston, TX, pp. 151-165, March 2013.

[38] J. Illingsworth, H. AI-Allak, and A. Brinkman, "Dependence of the Grain Boundary Potential Barrier Height of $BaTiO_3$ Ceramics on Donor Dopant Concentration." J. Phys. D: Appl. Phys., Vol. 23, no. 7, pp. 971-975, July 1990.